Syntheses and Optical Properties of Hybrid Materials Containing Azobenzene Groups via Sol–Gel Process for Reversible Optical Storage

Mi-Ra Kim,[1] Young-Il Choi,[1] Sang-Wook Park,[2] Jae-Wook Lee,[3] Jin-Kook Lee[1]

[1]*Department of Polymer Science and Engineering, Pusan National University, Pusan 609–735, South Korea*
[2]*Department of Chemical Engineering, Pusan National University, Pusan 609–735, South Korea*
[3]*Division of Chemical Engineering, Sogang University, Seoul 121–742, South Korea*

Received 30 March 2005; accepted 6 July 2005
DOI 10.1002/app.22355
Published online in Wiley InterScience (www.interscience.wiley.com).

ABSTRACT: We focused on the synthesis and optical properties of new organic–inorganic hybrid materials containing azobenzene groups for rewritable optical recording media. Hybrid material (SGUR19-*n*'s) design has the structure of azobenzene group with urethane bonds in the silica network. The structures of the synthesized monomers and precursors were confirmed by FTIR and ^{1}H NMR spectrophotometer. Also, we reported on the effects of the direction of the polarized beam, the intensity of the induced beam, and the structures of SGUR19-*n*'s materials on the diffraction efficiency of SGUR19-*n*'s films. It was revealed that SGUR19-*n*'s films prepared by the sol–gel process have adequate writing–erasing–rewriting properties when used as a reversible optical storage material. © 2006 Wiley Periodicals, Inc. J Appl Polym Sci 100: 4811–4818, 2006

Key words: hybrid materials; sol–gel process; diffraction efficiency; reversible optical storage materials

INTRODUCTION

During the last decade, organic–inorganic hybrid materials containing azobenzene groups and produced by the sol–gel process have been studied for use in optical data storage, nonlinear optical, and holographic applications.[1–7] The sol–gel process involving hydrolysis and condensation can form a variety of microstructures, such as matrices with high optical qualities at low temperatures. Also, the large variety of suitable organic molecules allows the optical, chemical, and mechanical properties to be controlled.[8] For optical information storage and erasing, as known, optically induced anisotropy in the azobenzene-containing material is required. When the film is irradiated with a linearly polarized laser beam, the photochemically induced trans–cis–trans photoisomerization of the azobenzene group within the film can generate photoinduced birefringence by reorienting of azobenzene molecules. Until recently, the materials were made from organic polymers as passive host matrices where active dye molecules such as methyl orange, methyl red, or disperse red 1 were introduced as guest units. These materials are cast onto a variety of substrates to provide thin films in which the doping molecules are either dispersed into[9] or grafted onto the polymer backbone.[10,11] Marino et al.[12] reported on the synthesis and holographic grating of disperse red 1-doped hybrid materials for optical storage materials.

In this study, we report on the synthesis and optical properties of three different hybrid materials (SGUR19-*n*'s) containing azobenzene units and diisocyanates produced by the sol–gel process. The materials were synthesized by the condensation reaction of disperse red 19 (DR 19) and three different diisocyanates in tetrahydrofuran, and then the sol–gel process is applied. Their optical properties and solubilities are compared with three structurally similar materials (SGUR19–1, SGUR19–2, and SGUR19–3). The diffraction efficiency and reversible photoinduced process of hybrid materials were measured as a function of reaction time. Additionally, the diffraction gratings of the hybrid materials were observed by atomic force microscopy (AFM).

EXPERIMENTAL

Materials

Disperse red 19 (DR 19), toluene-2,4-diisocyanate (2,4-TDI), toluene-2,6-diisocyanate (2,6-TDI), 4,4′-diphenylmethane diisocyanate, 3-(triethoxysilyl)propyl isocyanate (ICPTEOS), tetraethylortho silicate (TEOS), obtained from Aldrich Co., were used without further

Correspondence to: Mi-Ra Kim (mrkim2@pusan.ac.kr).
Contract grant sponsor: Basic Research Program of the Korea Science and Engineering Foundation through the Applied Rheology Center and Brain Korea 21.

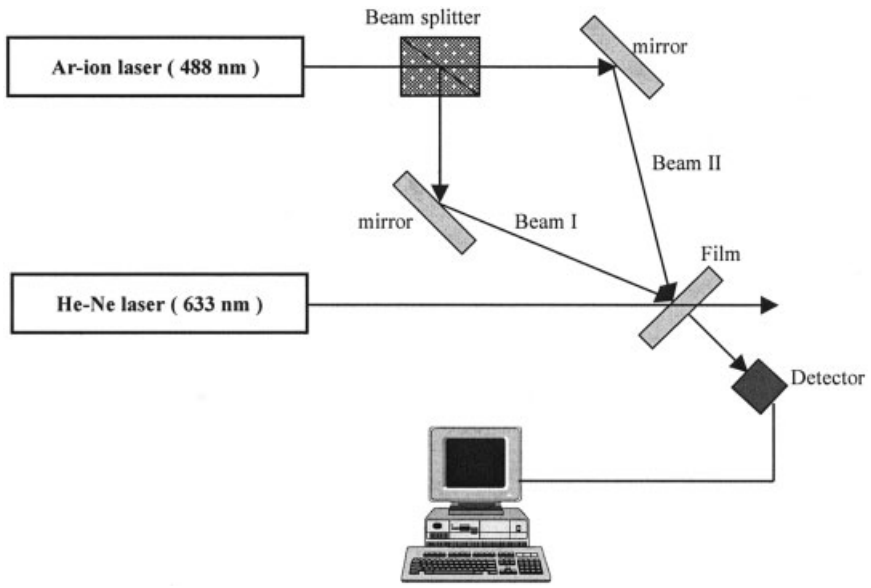

Figure 1 Experimental setup used to measure diffraction efficiency.

purification. *N,N′*-dimethylformamide (DMF), tetrahydrofuran (THF), dimethyl sulfoxide (DMSO), *n*-hexane and chloroform were used as received from Aldrich Co. Other chemicals were of reagent grade and were used without further purification.

Characterization

FTIR spectra were recorded using a JASCO 460 spectrophotometer. ^{1}H NMR spectra were recorded with a Varian Unity Plus 300 (300 MHz) spectrophotometer using tetramethylsilane (TMS) as an internal standard. UV–visible spectra were recorded using a UVIKON 860 spectrophotometer. Thermogravimetric analysis (TGA) was carried out on a Shimadzu TGA-50 in a nitrogen stream at a heating rate of 10°C/min.

Experimental setup and real-time dynamic holographic recording

The schematic diagram of the experimental setup is shown in Figure 1. A linearly polarized Ar^+ laser of 488 nm was used as the pump beam, and a He–Ne laser beam at 633 nm as the probe beam. The intensity of the probe beam was set to 1.0 mW/cm^2.

Real-time holographic recording was performed by employing two recording beams at 488 nm from an Ar+ laser. The interbeam angle was set to 11° in all of the experiments. The reading beam was set at 633 nm from a He–Ne laser. The continuous dynamic reading of the diffraction light with a photometer allowed synchronous observation of the diffraction efficiency. The diffraction efficiency (η) is defined as

$$\eta = I_d / I_i \quad (1)$$

where I_d is the intensity of the first-order diffracted beam, and I_i is the intensity of input beam.

Syntheses and characterizations of UR19-*n*'s and UR19T-*n*'s

A solution of DR19 (0.4 g, 1.211 mmol) and 2,4-toluene diisocyanate (2,4-TDI) (0.105 g, 0.605 mmol) in THF (10 mL) was heated to 70°C with vigorous stirring under nitrogen purge for 6 h. The reaction mixture was cooled to room temperature, and then poured into *n*-hexane. The resulting precipitates were reprecipitated into *n*-hexane and dried in a vacuum oven for 24 h. The product (UR19–1) was obtained as a dark red powder. UR19–1 (0.4 g, 0.479 mmol) and ICPTEOS (0.237 g, 0.958 mmol) in THF (10-mL) was heated to 70°C with vigorous stirring under nitrogen purge for 24 h. The reaction mixture was cooled to room temperature, and then poured into *n*-hexane. The resulting precipitates were reprecipitated into *n*-hexane and dried in a vacuum oven for 24 h. The product (UR19T-1) was also obtained as a dark red powder. The reaction routes of UR19-*n*'s and UR19T-*n*'s are illustrated in Figure 2. The synthesis of UR19T-2 and UR19T-3 followed the same procedures as described earlier, except that, toluene-2,6-diisocyanate and 4,4′-diphenylmethane diisocyanate were used as diisocyanates, respectively. The characterizations of UR19-*n*'s and UR19T-*n*'s as the structures were as follows:

Spectral data for (UR19–1): FTIR (THF solution, cm^{-1}), 3334 (NH and OH stretching), 1711 (C═O stretching), 1516 (NO_2 asym stretching), 1386 (NO_2 sym stretching), 1227 (C—N and C—O coupled stretching); ^{1}H NMR (DMSO-d_6, ppm), δ 8.93–8.81 (2H, —NH—), 8.23–8.21, 7.81–7.78 (8H, NO_2—aromatic—

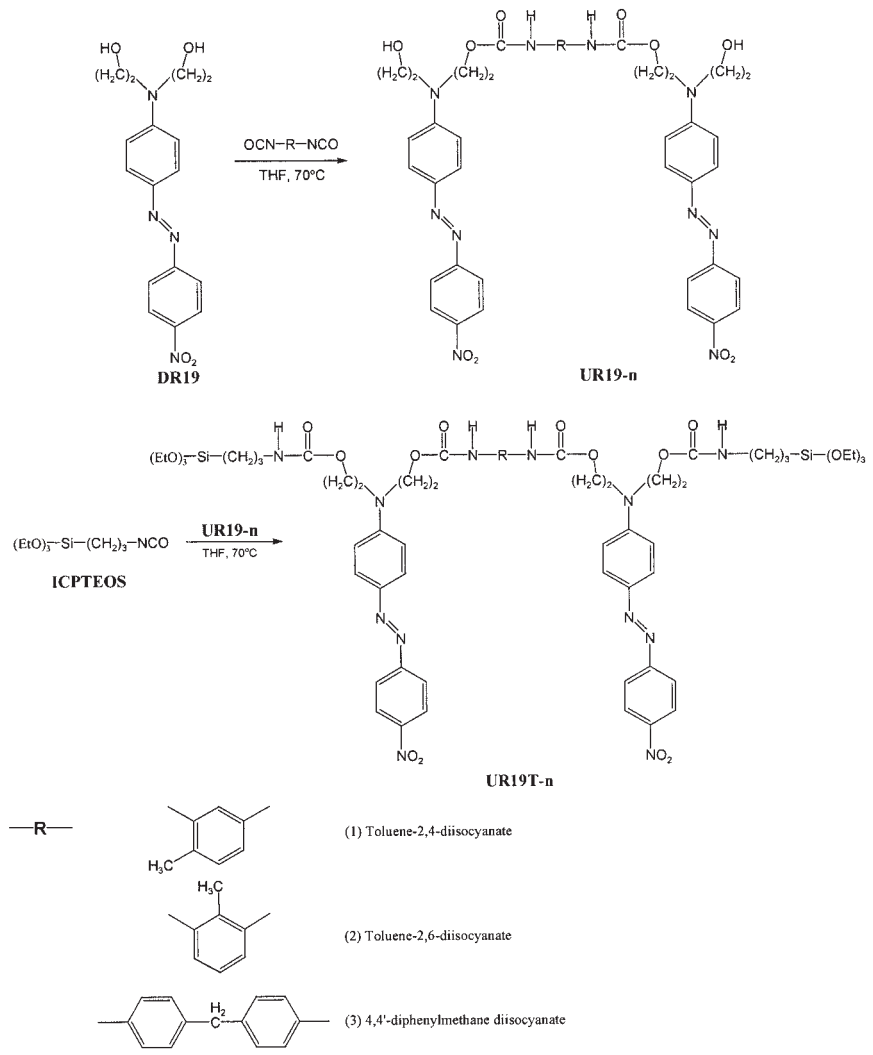

Figure 2 The synthetic routes and the structures of UR19-*n*'s and UR19T-*n*'s.

N═N—), 7.70–7.68, 6.79–6.77 (8H, —N═*N*—aromatic—N—), 7.38–6.85 (3H, aromatic), 4.78 (2H, —NCH_2CH_2OH), 4.16 (4H, —NCH_2CH_2O—), 3.69 (4H, —NCH_2CH_2OH), 3.47 (4H, —NCH_2CH_2O—), 3.47 (4H, —NCH_2CH_2OH), 2.06 (3H, —CH_3).

Spectra Data for (UR19–2): FTIR (THF solution, cm^{-1}), 3300 (NH and OH stretching), 1717 (C═O stretching), 1515 (NO_2 asym stretching), 1386 (NO_2 sym stretching), 1222 (C—N and C—O coupled stretching); ^1H NMR (DMSO-d_6, ppm), δ 8.89 (2H, —NH—), 8.23–8.21, 7.81–7.78 (8H, NO_2—aromatic—N═N—), 7.71–7.68, 6.79–6.76 (8H, —N═*N*—aromatic—N—), 6.96–6.82 (3H, aromatic), 4.78 (2H, —NCH_2CH_2OH), 4.15 (4H, —NCH_2CH_2O—), 3.67 (4H, —NCH_2CH_2OH), 3.47 (4H, —NCH_2CH_2O—), 3.47 (4H, —NCH_2CH_2OH), 1.85 (3H, —CH_3).

Spectra Data for (UR19–3): FTIR (THF solution, cm^{-1}), 3307 (NH and OH stretching), 1728 (C═O stretching), 1516 (NO_2 asym stretching), 1386 (NO_2 sym stretching), 1224 (C—N and C—O coupled stretching); ^1H NMR (DMSO-d_6, ppm), δ 9.48 (2H, —NH—), 8.24–8.21, 7.80–7.78 (8H, NO_2—aromatic—N═N—), 7.72–7.69, 6.85–6.80 (8H, —N═*N*—aromatic—N—), 7.20, 6.95 (8H, —aromatic—CH_2—aromatic—), 4.77 (2H, —NCH_2CH_2OH), 4.16 (4H, —NCH_2CH_2O—), 3.68–3.65 (4H, —NCH_2CH_2OH), 3.68–3.65 (2H, —aromatic—CH_2—aromatic—), 3.48 (4H, —NCH_2CH_2O—), 3.48 (4H, —NCH_2CH_2OH).

Spectra Data for (UR19T-1): FTIR (THF solution, cm^{-1}), 3336 (NH stretching), 1708 (C═O stretching), 1516 (NO_2 asym stretching), 1386 (NO_2 sym stretching), 1233 (C—N and C—O coupled stretching), 1077 (Si—O—C asym stretching), 956 (Si—O—C sym stretching); ^1H NMR (DMSO-d_6, ppm), δ 8.93–8.80 (2H, —NH—aromatic—), 8.23–8.21, 7.82–7.78 (8H, NO_2—aromatic—N═N—), 7.71–7.68, 6.82–6.79 (8H, —N═*N*—aromatic—N—), 7.38, 6.86–6.82 (3H, aromatic), 7.09 (2H, —NH—), 4.16 (8H, —NCH_2CH_2O—), 3.62–3.56 (8H, —NCH_2CH_2O—), 3.62–3.56 (12H, —Si—OCH_2CH_3), 2.79 (4H, —Si—$CH_2CH_2CH_2N$—), 2.06 (3H,

TABLE I
Reaction Molar Ratio for Syntheses of SGURI9-*n*'s

	SGUR19-*n* (*n* = 1, 2, 3)
DR-19	2
Diisocyanate[a]	1
ICPTEOS[b]	2
TEOS[c]	6
H_2O	32
HCl	0.208
DMF[d]	64

[a] *n* = l: toluene-2,4-diisocyanate(2,4-TDI); *n* = 2: toluene-2,6-diisocyanate (2,6-TDI); *n* = 3: 4,4′-diphenylmethane diisocyanate.
[b] 3-(Triethoxysilyl)propyl isocyanate.
[c] Tetraethyl orthosilicate.
[d] *N,N*′-Dimethylformamide.

—CH_3), 1.31–1.25 (4H, —Si—$CH_2CH_2CH_2N$—), 1.01–0.95 (18H, —Si—OCH_2CH_3), 0.40–0.35 (4H, —Si—$CH_2CH_2CH_2N$—).

Spectra Data for (UR19T-2): FTIR (THF solution, cm^{-1}), 3321 (NH stretching), 1717 (C═O stretching), 1516 (NO_2 asym stretching), 1386 (NO_2 sym stretching), 1234 (C—N and C—O coupled stretching), 1077 (Si—O—C asym stretching), 956 (Si—O—C sym stretching); ^{1}H NMR (DMSO-d_6, ppm), δ 8.87 (2H, —NH—aromatic—), 8.21–8.19, 7.79–7.77 (8H, NO_2—aromatic—N═N—), 7.70–7.68, 6.79–6.76 (8H, —N═*N*—aromatic—N—), 7.09 (2H, —NH—), 6.85–6.82 (3H, —aromatic—), 4.14 (8H, —NCH_2CH_2O—), 3.64–3.56 (12H, —Si—OCH_2CH_3), 3.50–3.46 (8H, —NCH_2CH_2O—), 2.79 (4H, —Si—$CH_2CH_2CH_2N$—), 1.83 (3H, —CH_3), 1.31–1.25 (4H, —Si—$CH_2CH_2CH_2N$—), 1.01–0.95 (18H, —Si—OCH_2CH_3), 0.39–0.35 (4H, —Si—$CH_2CH_2CH_2N$—).

Spectra Data for (UR19T-3): FTIR (THF solution, cm^{-1}), 3320 (NH stretching), 1719 (C═O stretching), 1516 (NO_2 asym stretching), 1386 (NO_2 sym stretching), 1227 (C—N and C—O coupled stretching), 1076 (Si—O—C asym stretching), 956 (Si—O—C sym stretching); ^{1}H NMR (DMSO-d_6, ppm), δ 9.48 (2H, —NH—aromatic—), 8.22, 7.79 (8H, NO_2—aromatic—N═N—), 7.69, 6.85–6.80 (8H, —N═*N*—aromatic—N—), 7.18,6.94 (8H, —aromatic—CH_2—aromatic—), 7.09 (2H, —NH—), 4.14 (8H, —NCH_2CH_2O—), 3.68–3.54 (2H, —aromatic—CH_2—aromatic—), 3.68–3.54 (12H, —Si—OCH_2CH_3), 3.47 (8H, —NCH_2CH_2O—), 2.78 (4H, —Si—$CH_2CH_2CH_2N$—), 1.31–1.25 (4H, —Si—$CH_2CH_2CH_2N$—), 1.01–0.95 (18H, —Si—OCH_2CH_3), 0.39–0.35 (4H, —Si—$CH_2CH_2CH_2N$—).

Sol–gel process and film preparation

The products (UR19T-*n*'s) were dissolved in DMF, and each solution was mixed with tetraethylortho silicate (TEOS) at room temperature for 10 min. Then, the mixture of water and HCl was added drop-wise for 30 min. The solution was hydrolyzed and condensed at room temperature for 90 min. The total molar ratios of the reactions are shown in Table I.

For studying the optical properties, we fabricated a thin film. The sol was filtered with a 0.2-μm nylon filter and spin-coated onto a clean glass slide at 1000 rpm. The coated glass pieces were dried in a vacuum oven at 80°C for 2 h. The thickness of the films, measured by a Dektak3 (α-step), were about 1.39, 1.02, and 1.5 μm for SGUR19–1, SGUR19–2, and SGUR19–3, respectively

RESULTS AND DISCUSSION

Syntheses and characterizations of SGUR19-*n*'s

SGUR19-*n*'s containing azobenzene group was fabricated using the sol–gel process of TEOS and UR19T-*n*'s. The chemical structures of UR19-*n*'s and UR19T-*n*'s are shown in Figure 2. The structures of synthesized UR19-*n*'s and UR19T-*n*'s were confirmed by FTIR and ^{1}H NMR spectroscopy. The FTIR spectra of UR19-*n*'s showed characteristic absorption peaks at 1728–1711 cm^{-1} due to C═O stretching of the urethane group, and 1227–1222 cm^{-1} due to C—N and C—O coupled stretching of the urethane group. The FTIR spectra of UR19T-*n*'s showed characteristic absorption peaks at 1719–1708 cm^{-1} due to C═O stretching of the urethane group, 1234–1227 cm^{-1} due to C—N and C—O coupled stretching of the urethane group, and 1077 and 956 cm^{-1} due to Si—O—C asym and sym stretching of the ICPTEOS, respectively. The ^{1}H NMR spectrum of UR19–1 exhibited characteristic peaks at δ 8.93–8.81 ppm assignable to the *N*—H of the urethane linkage, δ 8.23–6.77 ppm assignable to aromatic group of the azobenzene, and δ 7.38–6.85 ppm for the diisocyanate.

TABLE II
Solubilities of UR19T-*n*'s with Different Diisocyanates

	Hexane	Methanol	Ethanol	Chloroform	Acetone	THF	DMF	DMSO
UR19T-1	×	•	•	•	•	•	•	•
UR19T-2	×	•	•	•	•	•	•	•
UR19T-3	×	•	•	•	•	•	•	•

×: Insoluble; •: soluble.

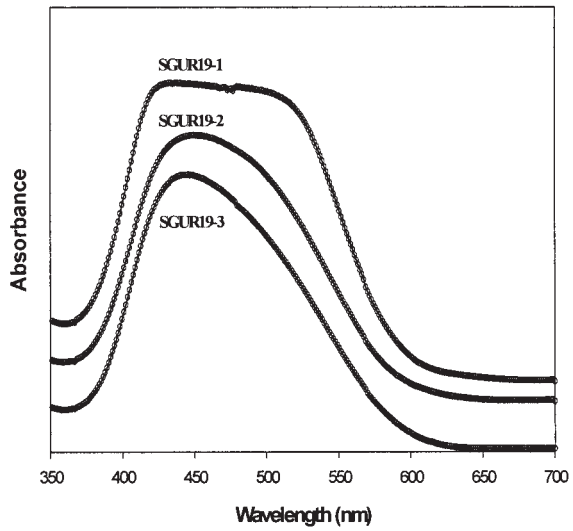

Figure 3 UV–vis absorption spectra of SGUR19-*n*'s films.

The solubilities of different UR19T-*n*'s are summarized in Table II. The UR19T-*n*'s were only insoluble in hexane, whereas they were readily soluble in common organic solvents or aprotic solvents such as *N*,*N*-dimethylformamide (DMF) and dimethyl sulfoxide (DMSO). The UV–vis absorption spectra of SGUR19-*n*'s are shown in Figure 3. The absorption spectra of SGUR19–1, SGUR19–2, and SGUR19–3 had maximum of 446, 450, and 433 nm, respectively.

The thermal properties of the SGUR19-*n*'s were determined by differential scanning calorimetry (DSC) and thermogravimetric analysis (TGA). The glass-transition temperature (T_g) and the initial decomposition temperature (T_d) of SGUR19-*n*'s are summarized in Table III. The T_g's of SGUR19–1, SGUR19–2, and SGUR19–3 were observed at 160.4, 152.0, and 147.0°C, respectively. The relatively high T_g of SGUR19-*n*'s is attributed to the silica network structure containing aromatic ring in the main chain and conjugated aromatic ring in the side chain. The initial decomposition temperature (T_d) results are also summarized in Table III. For SGUR19-*n*'s, the T_d's of SGUR19–1, SGUR19–2, and SGUR19–3 were observed at 410, 395, and 393°C, respectively. Regardless of the structure of diisocyanates, SGUR19-*n*'s were relatively thermally stable.

TABLE III
Glass-Transition Temperatures (T_g's) and Initial Thermal Decomposition Temperatures (T_d's) of SGUR19-*n*'s with Different Diisocyanate Structures

	T_g (°C)[a]	T_d (°C)[b]
SGUR19–1	160.4	410
SGUR19–2	152.0	395
SGUR19–3	147.0	393

[a] DSC thermogram data on the second heating, at a heating rate of 10°C/min.
[b] TGA measurements at a heating rate of 10°C/min (nitrogen atmosphere).

Effect of intensity of induced laser beam on diffraction efficiency for SGUR19-*n*'s

To investigate the optimum condition of the induced laser beam, we measured the diffraction efficiency as the intensity of the induced laser beam for SGUR19-*n*'s films. The probe beam used a He–Ne laser beam at 633 nm. An Ar^+ laser beam at 488 nm was induced with intensities of 10, 25, and 40 mW/cm^2. Figure 4 shows that when the laser beam was turned on, the diffraction efficiency rapidly increased, saturated, and remained at the level of almost 0.78% (40 mW/cm^2). In

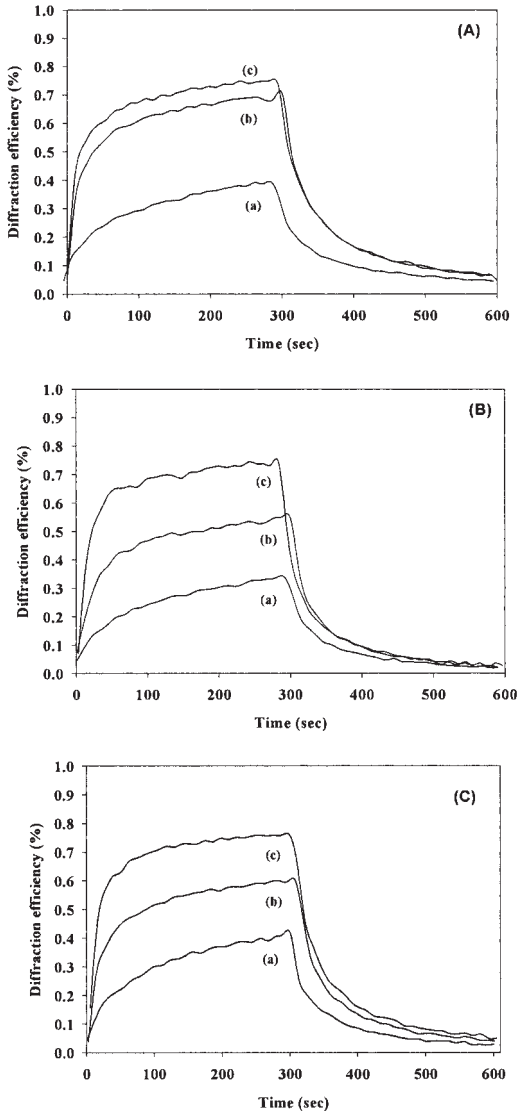

Figure 4 Diffraction efficiency as a function of time for SGUR19–1 (A), SGUR19–2 (B), and SGUR19–3 (C) at different intensities of induced laser beam: 10 mW/cm^2 (a), 25 mW/cm^2 (b), 40 mW/cm^2 (c).

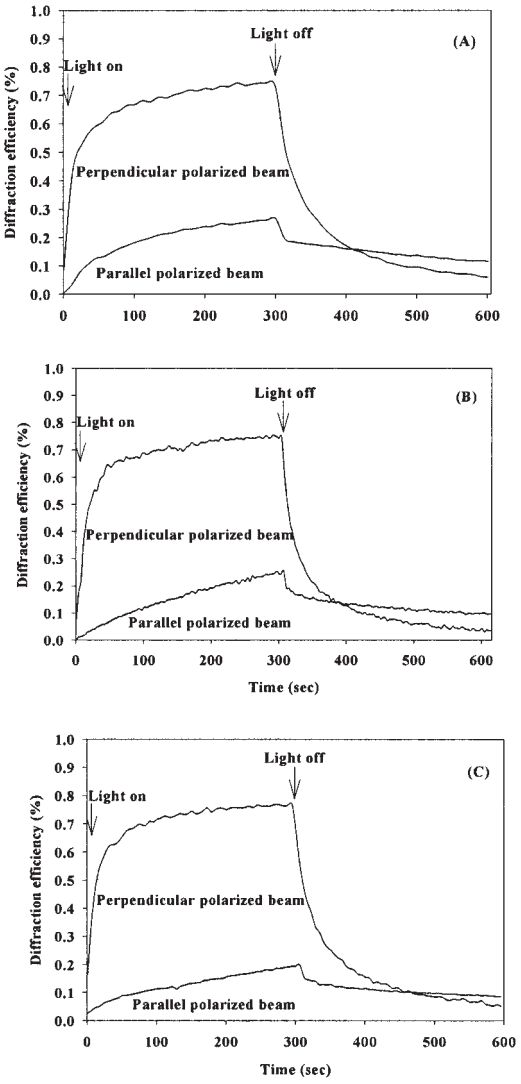

Figure 5 Diffraction efficiency as a function of time for SGUR19–1 (A), SGUR19–2 (B), and SGUR19–3 (C) in the direction of polarized laser beams at 40 mW/cm^2 (perpendicular- or parallel-polarized beams).

all films, independent of their chemical structures, as the intensity of the laser beam increased, the maximum diffraction efficiency also increased. In our previous study,[13] because the high intensity of the induced laser beam caused damage to the polymer film, the diffraction efficiency decreased. However, in this study, there is no film damage because of the thermal stability of hybrid materials containing silica network structure.

Diffraction efficiency of scalar hologram and vector hologram for SGUR19-*n*'s

To research reversible recording by the photoisomerization, we used an optical setup as shown in Figure 1. An Ar^+ laser at 488 nm, which is the most absorbable wavelength for the SGUR19-*n*'s film, was used as a light source. The source beam was separated with a beam splitter, and they overlapped on the surface of the film. If the two separated beams were parallel to the polarization (90°and 90°), a scalar hologram was obtained. If they were perpendicular (90°and 0°), then a vector hologram was obtained. The diffraction efficiency as a function of time in a scalar hologram and vector hologram at 40 mW/cm^2 for SGUR19–1 (A), SGUR19–2 (B), and SGUR19–3 (C) is shown in Figure 5. Figure 5 shows the initial diffraction efficiency of SGUR19-*n*'s for the vector hologram (perpendicular polarized beams) and the scalar hologram (parallel polarized beams). The initial diffraction efficiency of the film in the vector hologram was higher than that of the film in the scalar hologram. At the film's maximum diffraction efficiency, SGUR19–1 has maximum diffraction efficiencies of 0.76% (vector) and 0.27%

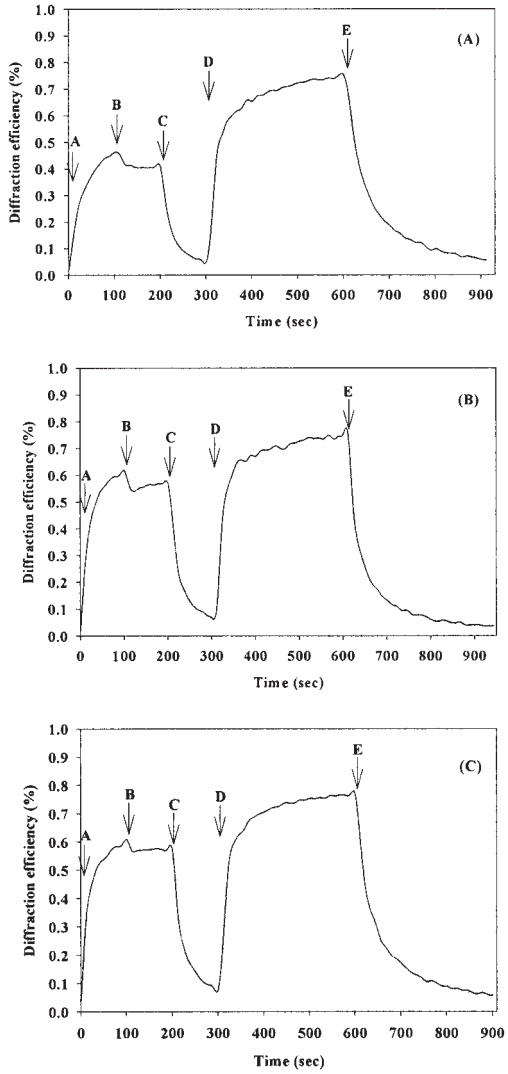

Figure 6 Writing–erasing curves of SGUR19–1 (A), SGUR19–2 (B), and SGUR19–3 (C) film at 40mW/cm^2 (A,D: two beams turn on; B: two beams turn off; and C,E: only one beam turn on).

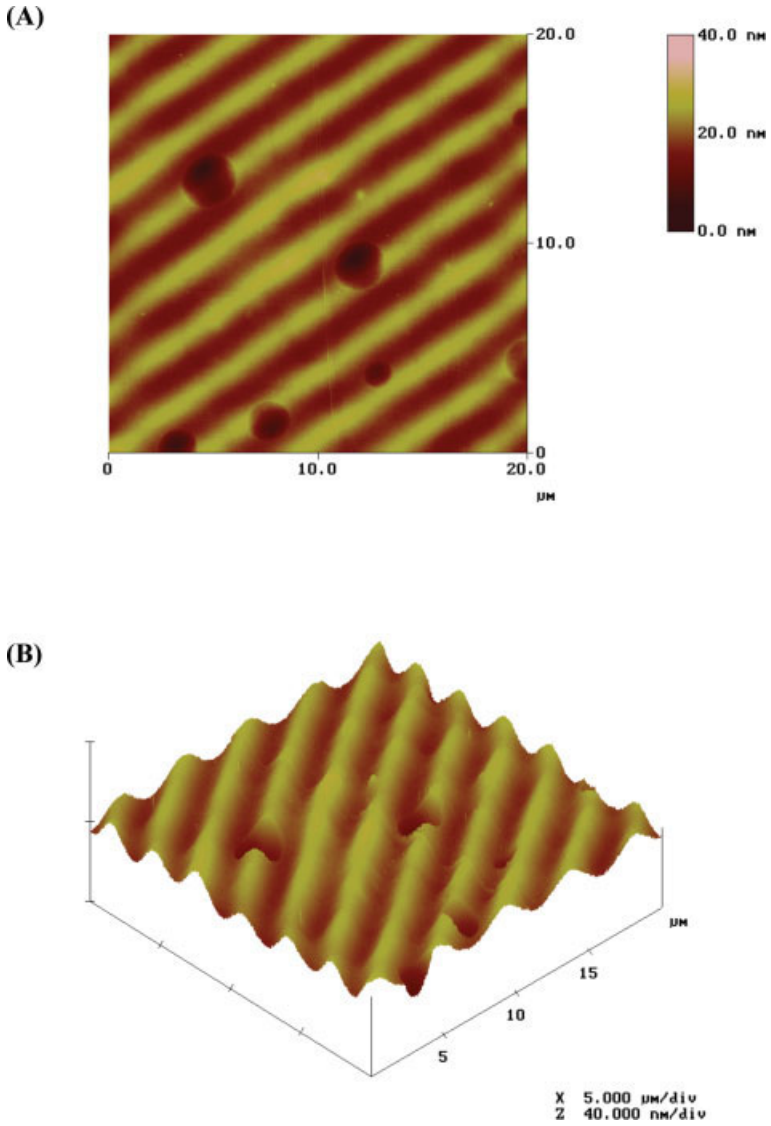

Figure 7 2D (A) and 3D (B) AFM views of the surface relief gratings on SGUR19–1 film. [Color figure can be viewed in the online issue, which is available at www.interscience.wiley.com.]

(scalar). Similar results were shown for SGUR19–2 and SGUR19–3. SGUR19–2 has maximum diffraction efficiencies of 0.76% (vector) and 0.26% (scalar). SGUR19–3 has maximum diffraction efficiencies of 0.78% (vector) and 0.20% (scalar). The vector hologram with different polarization direction beam induces cis–trans photoisomerization of the azobenzene group in the silica network. Namely, the vector hologram is formed by pure beam polarization interference. The scalar hologram with the same polarization direction beam induces the macroscopic movement of the organic chain in the silica network. In contrast to the vector hologram, the scalar hologram is formed by pure beam intensity interference. Therefore, the cis–trans photoisomerization by the vector hologram responds to the induced laser more quickly than the macroscopic movement of the organic chain in the silica network by the scalar hologram.

Write–erase processing for SGUR19-*n*'s

We investigated diffraction efficiency as a function of time for SGUR19-*n*'s films during the recording process. An Ar^+ laser beam at 488 nm with an intensity of 40 mW/cm^2 was used. As the orientation grating was formed, the diffraction efficiency increased, saturated, and remained at a constant value throughout the rest of the recording process. When the writing beam was turned on, the diffraction efficiency increased rapidly and reached 0.76, 0.76, and 0.78%. After one beam was turned off, the diffraction efficiency decayed to nearly zero, indicating that most of the orientation grating had been erased. The structural differences of the hybrid films by the diisocyanate group did not have an effect on diffraction efficiency. Figure 6 gives a typical first write–erase and second write–erase profile of optically induced diffraction efficiency for the

SGUR19-*n*'s with an intensity of 40 mW/cm^2. At point A, the two linearly polarized writing beams are turn on and diffraction efficiency increases. The two writing beams are turned off at point B, and relaxation occurs to a stable level at point C. When one beam is turned on, erasing is started at point C. The second writing–erasing is also performed in the same manner. At point D, the two writing beams are turned on, and one beam is turned off at point E. The results show that the second writing rate is faster than the first one; however, the second one erases slower than first one.

Surface relief grating of SGUR film

Surface relief grating with large surface modulations could be formed on the hybrid material with azobenzene group. Figure 7 shows a typical atomic force microscopy (AFM, Nanoscope III A, Digital Instrument Co.) view of the surface relief gratings formed on a SGUR19–1 film. The gratings were fabricated using simple interference of the two linearly polarized 488 nm beams from an Ar^+ laser with an intensity of 25 mW/cm^2 as the pump beam. A He–Ne laser at 633 nm, used as the probe beam, was inputted at an intensity of 1.0 mW/cm^2. The grating spacing was controlled by changing the angle between the two beams. AFM view of the surface relief grating on the SGUR19–1 showed a depth of 15 nm and a surface distance of 2.50 μm.

CONCLUSIONS

We have synthesized SGUR19-*n*'s (SGUR19–1, SGUR19–2, and SGUR19–3) containing an azobenzene group by the condensation reaction between DR 19 and three different diisocyanates and by the sol–gel process. The UR19T-*n*'s were very soluble in common organic solvents or aprotic solvent. The diffraction efficiency of the SGUR19-*n*'s film was measured as a function of the reaction time. The diffraction efficiency of SGUR19–1, SGUR19–2, and SGUR19–3 film at 40 mW/cm^2 was observed up to a level of 0.76, 0.76, and 0.78%, respectively. Independent of the film's structure, as the intensity of the laser beam increased, the maximum diffraction efficiency also increased. In contrast to our past study, the film was not damaged, because hybrid materials containing silica network structure have good thermal stability. The vector hologram induces the cis–trans photoisomerization of the azobenzene group in the silica network, and the scalar hologram with the same polarization direction beam induces the macroscopic movement of the organic chain in the silica network. The cis–trans photoisomerization by the vector hologram responded to the induced-laser more quickly than the macroscopic movement of the organic chain in the silica network by the scalar hologram. The SGUR19-n's showed adequate writing–erasing–rewriting properties and a fairly stable diffraction level when used as a reversible optical storage material.

References

1. Raschellà, R.; Marino, I. G.; Lottici, P. P.; Bersani, D.; Lorenzi, A.; Montenero, A. Opt Mat 2004, 25, 419.
2. Rosso, V.; Loicq, J.; Renotte, Y.; Lion, Y. J Non-Crys Sol 2004, 342, 140.
3. Marino, I. G.; Bersani, D.; Lottici, P. P. Opt Mat 2001, 15, 279.
4. Muto, S.; Kubo, T.; Kurokawa, Y.; Suzuki, K. Thin Solid Film 1998, 322, 233.
5. Riehl, D.; Chaput, F.; Lévy, Y.; Boilot, J.-P.; Kajzar, F.; Chollet, P.-A. Chem Phys Lett 1995, 245, 36.
6. Chaput, F.; Riehl, D.; Lévy, Y.; Boilot, J. P. Chem Mater 1993, 5, 589.
7. Novak, B. M. Adv Mater 1993, 5, 422.
8. Hsiue, G. H.; Kuo, W. H.; Lin, C. H.; Jeng, R. J Macromol Chem Phys 2000, 201, 2336.
9. Luckemeyer, T.; Franke, H. Appl Phys Lett 1988, 53, 2017.
10. Natansohn, A.; Rochon, P.; Gosselin, J.; Xie, S. Macromolecules 1992, 25, 2268.
11. Shi, Y.; Steier, W. H.; Yu, L.; Chen, M.; Dalton, R. Appl Phys Lett 1991, 58, 1131.
12. Marino, I. G.; Bersani, D.; Lottici P. P. Opt Mat 2000, 15, 175.
13. Kim, M. R.; Kim, P. S.; Kang, E. H.; Ha, C. S.; Lee, J. K. Polym Int 2003, 52, 658.